

# RGMIM: Region-Guided Masked Image Modeling for Learning Meaningful Representation from X-Ray Images

Guang Li<sup>a</sup>, Ren Togo<sup>b</sup>, Takahiro Ogawa<sup>b</sup>, Miki Haseyama<sup>b</sup>

<sup>a</sup>Graduate School of Information Science and Technology, Hokkaido University,  
N-14, W-9, Kita-Ku, Sapporo, 060-0814, Japan

<sup>b</sup>Faculty of Information Science and Technology, Hokkaido University,  
N-14, W-9, Kita-Ku, Sapporo, 060-0814, Japan

## Abstract

*Purpose:* Self-supervised learning has been gaining attention in the medical field for its potential to improve computer-aided diagnosis. One popular method of self-supervised learning is masked image modeling (MIM), which involves masking a subset of input pixels and predicting the masked pixels. However, traditional MIM methods typically use a random masking strategy, which may not be ideal for medical images that often have a small region of interest for disease detection. To address this issue, this work aims to improve MIM for medical images and evaluate its effectiveness in an open X-ray image dataset.

*Methods:* In this paper, we present a novel method called region-guided masked image modeling (RGMIM) for learning meaningful representation from X-ray images. Our method adopts a new masking strategy that utilizes organ mask information to identify valid regions for learning more meaningful representations. The proposed method was contrasted with five self-supervised learning techniques (MAE, SKD, Cross, BYOL, and, SimSiam). We conduct quantitative evaluations on an open lung X-ray image dataset as well as masking ratio hyperparameter studies.

*Results:* When using the entire training set, RGMIM outperformed other comparable methods, achieving a 0.962 lung disease detection accuracy. Specifically, RGMIM significantly improved performance in small data volumes, such as 5% and 10% of the training set (846 and 1,693 images) compared to other methods, and achieved a 0.957 detection accuracy even when only 50% of the training set was used.

*Conclusions:* RGMIM can mask more valid regions, facilitating the learning of discriminative representations and the subsequent high-accuracy lung disease detection. RGMIM outperforms other state-of-the-art self-supervised learning methods in experiments, particularly when limited training data is used. With the help of the Segment Anything Model, RGMIM also has the potential to be applied to different modalities of medical images.

*Keywords:* Self-supervised learning, Masked image modeling, Segment anything model, X-ray images.

## 1. Introduction

Self-supervised learning is regarded as the most essential part of artificial intelligence and has made great progress in the medical field [1, 2, 3]. Early self-supervised learning techniques usually learn representations through a simple prior task that applies transformations such as rotate [4] and jigsaw puzzle [5] to the input image and make the model predict the properties of the transformation from the transformed image. Afterward, contrastive learning methods have been demonstrated to be efficient on different tasks [6]. These approaches aim to make the distances between various view representations enhanced from the same image (i.e., positive sample pairs) closer while making the distances between view representations enhanced from

different images (i.e., negative sample pairs) farther [7]. Nevertheless, as these techniques depend on data augmentation, the hyperparameters and data augmentation strategies need to be changed frequently [8].

As one of the hot research topics of self-supervised learning, masked image modeling (MIM) has recently attracted more and more attention [9, 10, 11]. In the discipline of natural language processing, masked language modeling (MLM) is a task that masks a portion of the input pixels and tries attempts to predict the masked pixels [12]. Accordingly, recovering a large number of masked patches from a small number of unmasked patches allows the model to learn sufficient semantic information [13]. In comparison to contrastive learning techniques relying on significant data augmentation, MIM is also more straightforward and reliable. As a result, it is valuable to investigate the role of MIM on real-world datasets such as medical image datasets [14].

Traditional MIM techniques frequently employ a random masking strategy for ordinary images [10]. Medical images,

Email addresses: guang@lmd.ist.hokudai.ac.jp (Guang Li<sup>a</sup>),  
togo@lmd.ist.hokudai.ac.jp (Ren Togo<sup>b</sup>),  
ogawa@lmd.ist.hokudai.ac.jp (Takahiro Ogawa<sup>b</sup>),  
mhaseyama@lmd.ist.hokudai.ac.jp (Miki Haseyama<sup>b</sup>)

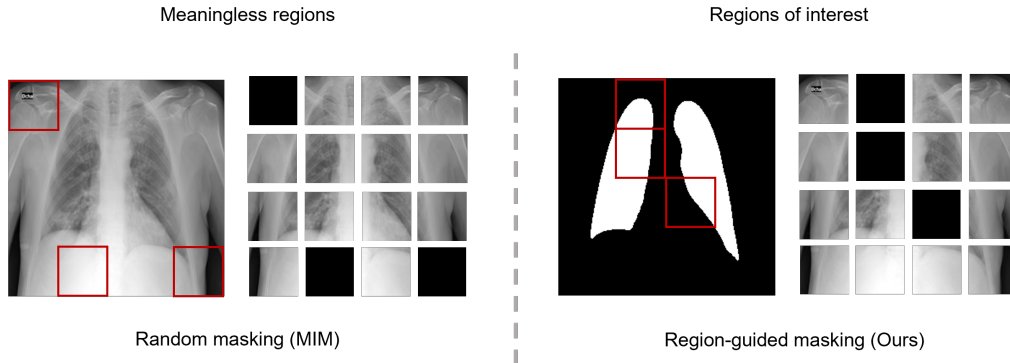


Figure 1: Comparison of the random masking and the proposed region-guided masking.

in comparison to ordinary images, often exhibit a smaller region of interest for disease detection [15]. For instance, when applied to lung disease detection, the regions outside the lung may not have the information needed to make a judgment, which could prevent the random masking strategy from learning enough information.

In this paper, we propose a novel method called region-guided masked image modeling (RGMIM) for learning meaningful representation from X-Ray images. Our approach is designed to address the issue that medical images often have a smaller region of interest compared to ordinary images, by using organ mask information to identify valid regions for learning more useful information. Specifically, we introduce a new masking strategy in our method. As depicted in Fig. 1, the proposed region-guided masking strategy can resolve the shortcomings of random masking in medical images. RGMIM obtained a 0.962 lung disease detection accuracy on an open X-ray image dataset according to experimental results. When limited training data was used, RGMIM drastically outperformed other state-of-the-art (SOTA) self-supervised learning methods significantly.

Moreover, leveraging the recently proposed Segment Anything Model (SAM) [16] can facilitate the extension of RGMIM to various modalities of medical images beyond X-ray. The acquisition of ground truth mask images can be a major challenge in the application of RGMIM to other medical image modalities. However, this challenge can be overcome by utilizing SAM to obtain the region of interest without requiring the corresponding ground truth mask images. Our main contributions are listed as follows:

- We propose a novel RGMIM for learning meaningful representation from X-ray images.
- RGMIM significantly outperforms other SOTA self-supervised learning methods on an open X-ray dataset, especially when using limited training data.
- We explore the possibility of applying SAM to RGMIM and demonstrate the potential of RGMIM for different modalities of medical images.

The next of the paper is organized as follows. First, we show some related works in Section 2. Then, we depict the details of

the proposed method in Section 3. Next, we show the experimental settings and results in Section 4. Finally, we conduct discussions and conclusions in Sections 5 and 6, respectively.

## 2. Methods

### 2.1. Self-Supervised Learning

In recent years, self-supervised learning has emerged as a powerful paradigm in machine learning, enabling models to acquire knowledge from unlabeled data without explicit annotations [17]. Self-supervised learning has gained significant attention due to its potential to leverage abundant unlabeled data that is freely available and to mitigate challenges related to data scarcity and labeling costs across various domains. Within the field of self-supervised learning, we mainly focus on two hot topics: contrastive learning and masked image modeling.

One widely adopted technique in self-supervised learning is contrastive learning [6], which aims to learn representations by contrasting positive pairs against negative pairs in a latent space. The InfoMax [18] principle proposed by Hjelm et al. provided an early theoretical framework for contrastive learning, which encourages models to maximize the mutual information between different views of the same input while minimizing the mutual information between the views of different inputs. Building upon the InfoMax principle, recent studies have proposed various algorithms to enhance the effectiveness of contrastive learning. For example, SimCLR [7] introduced a framework for training deep neural networks using large-batch contrastive learning. MoCo [19] introduced a memory bank to store negative examples and utilized a momentum encoder to update the model’s representations. BYOL [20] introduced a self-supervised learning method that does not require negative samples during training, which leverages two augmented views of input and employs a target network to create a moving average of the online network’s parameters, enabling more stable and efficient learning. Moreover, SimSiam [21] further simplifies the contrastive learning framework by using a fully symmetric Siamese network.

Masked image modeling is another prominent technique within the literature of self-supervised learning, involving the prediction of missing parts of an image based on contextual

cues [22]. The concept of masked language modeling gained substantial attention with the introduction of the popular BERT model [12] in the natural language processing domain. Inspired by BERT, some studies have extended the concept to the computer vision domain, enabling the extraction of meaningful representations from images by predicting missing regions. For example, BEiT [9] utilizes a mask-then-predict strategy to train the model, using target visual tokens generated by a readily available tokenizer. The tokenizer is pretrained using a discrete variational autoencoder [23], effectively making BEiT a two-stage training process resembling a denoising autoencoder [24]. This approach of BEiT involves separating masked prediction from autoencoder training, allowing for potential improvements in effectiveness and efficiency. In line with this objective, MAE [10] conducts experiments involving end-to-end training of a masked autoencoder. In their proposed method, MAE directly predicts masked patches from the unmasked ones, employing a simple mean squared error (MSE) loss. Notably, the masking ratio is set at 75%, significantly higher than the ratios used in BERT (typically 15%) or prior MIM approaches (ranging from 20% to 50%) [25, 26, 9]. Concurrently, a similar architecture called Simple Masked Image Modeling (SimMIM) is introduced in [11], which corroborates the findings of MAE. Specifically, SimMIM demonstrates that directly predicting the pixels, as done in MAE, performs no worse than other methods with more complex designs involving tokenization, clustering, or discretization.

## 2.2. Representation Learning for Medical Images

Representation learning has emerged as a powerful approach in the field of medical images, enabling automated analysis, diagnosis, and treatment planning [27, 15]. Medical images, such as X-Ray images [28], CT scans [29], MRI scans [30], and histopathology slides [31], contain rich and complex information that can be challenging to interpret and analyze manually. Representation learning techniques aim to automatically extract meaningful and high-level representations from raw medical image data, facilitating the development of more accurate and efficient computer-aided diagnosis systems [32]. Traditionally, handcrafted features were used in medical image analysis, where experts would design specific features based on their knowledge of the anatomical structures and pathological characteristics [33]. However, this process is time-consuming, relies heavily on expert knowledge, and may not capture the full complexity and subtle patterns present in medical images. In recent years, representation learning methods, especially deep learning approaches, have revolutionized medical image analysis by automatically learning hierarchical representations directly from the data [34]. Deep convolutional neural networks, vision transformers, and generative models, such as variational autoencoders and generative adversarial networks, have shown great success in extracting meaningful features and representations from medical images [35].

Representation learning methods have the capability to leverage large-scale datasets, enabling them to learn robust and highly generalizable features from medical images [36]. The availability of substantial amounts of data plays a crucial role

in training these models to capture the intricate patterns and complexities present in medical images [37]. By training on diverse and extensive datasets, representation learning models can extract features that are applicable across various imaging modalities, patient populations, and clinical settings [38]. The utilization of large-scale datasets allows representation learning models to learn from a wide range of examples, encompassing the inherent variations and complexities encountered in real-world medical scenarios [39]. Furthermore, recent advances in self-supervised representation learning have shown promise in the field of medical image analysis [40]. For example, contrastive learning and masked image modeling, have been applied to learn representations from unlabeled medical images [41, 42]. Self-supervised learning allows models to learn from vast amounts of unlabeled medical data and have the potential to improve performance on downstream tasks such as lesion detection and disease classification [43, 44]. This capability is particularly valuable in scenarios where labeled data is limited or scarce [45, 46].

## 3. Methods

RGMIM is a pretraining task that uses Vision Transformer (ViT) to compare the original patches and the reconstructed masked patches. The network structure contains a ViT encoder and a ViT decoder. The ViT encoder transforms the unmasked lung X-ray patches into a latent representation. From the latent representation, the ViT decoder can reconstruct masked lung X-ray patches. An overview of RGMIM is shown in Fig. 2. The left indicates the pipeline and the right show the structure of the ViT encoder. RGMIM consists of five steps: (1) splitting the input lung X-ray image into patches, (2) matching the patches with the lung mask image, (3) masking some valid patches, (4) embedding the unmasked patches, and (5) compare the reconstructed patches and masked patches. In the following subsections, we go over the region-guided masking strategy, ViT encoder and decoder, pretraining process, fine-tuning, and lung disease detection in detail.

### 3.1. Region-Guided Masking Strategy

First, given an input lung X-ray image  $X \in \mathbb{R}^{H \times W \times C}$ , we divide it into  $n$  patches  $X_N \in \mathbb{R}^{n \times (T^2 \times C)}$ , where  $(H, W)$  denotes the size of the original lung X-ray image,  $C$  denotes the number of channels,  $(T, T)$  denotes the size of splitted patches, and  $n = HW/T^2$  is the number of patches. For ordinary images, traditional MIM methods frequently employ a random masking strategy. However, lung disease detection is only related to lung characteristics, and information from areas other than the lungs is meaningless. As shown on the left of Fig. 1, if we use a random masking strategy for lung X-ray images, we may mask too many ineffective areas (e.g., areas outside the lungs), and thus the self-supervised learning process cannot learn sufficient representations.

To tackle the aforementioned challenge, a novel masking strategy that utilizes lung mask information to identify the valid regions for learning more informative features for lung disease

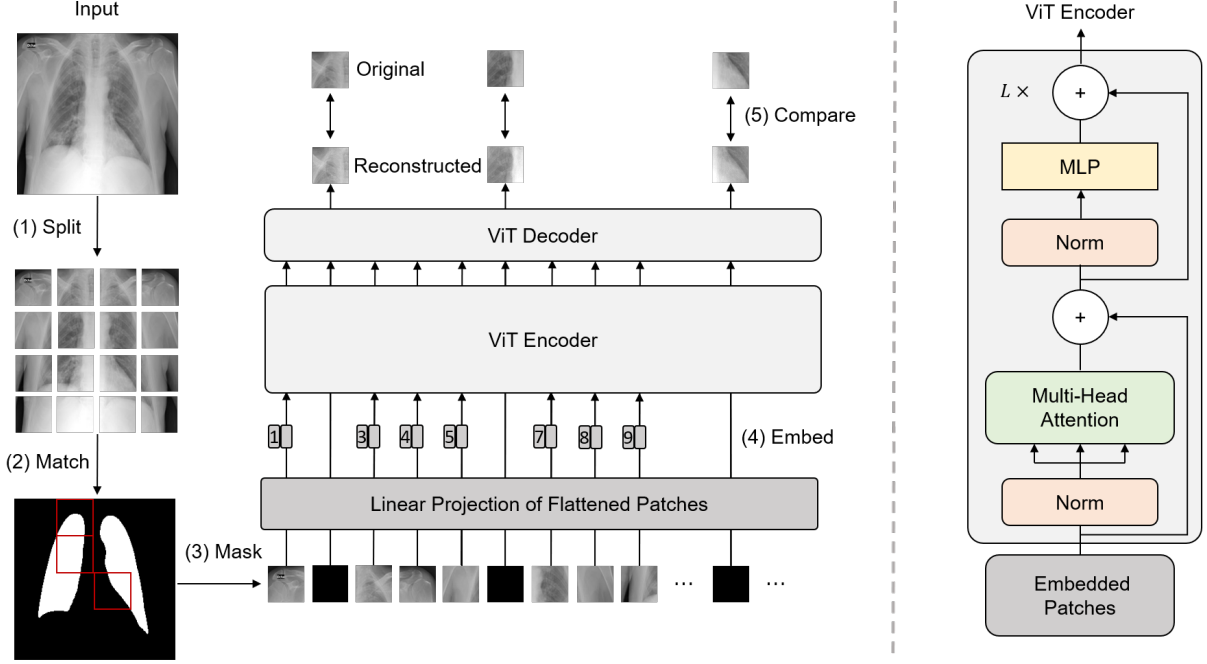


Figure 2: Overview of RGMIM. The left indicates the pipeline and the right show the structure of the ViT encoder.

detection is proposed in this study. For example, for each input lung X-ray image  $X$ , there is a corresponding lung mask image that represents the lung region. And we match the split patches  $X_N$  with the lung mask image. We define split patches as valid lung X-ray patches if they overlap with the lung mask image. Then we randomly mask  $m = n \times \sigma$  valid lung X-ray patches  $X_M$  with the masking ratio  $\sigma$  and obtain the remaining  $u = n \times (1 - \sigma)$  unmasked patches  $X_U$ . The unmasked patches  $X_U$  served as the effective input sequence of the ViT encoder. With the proposed region-guided masking strategy, we can mask more valid lung-related regions, facilitating the learning of discriminative representations and the subsequent high-accuracy lung disease detection.

### 3.2. ViT Encoder and Decoder

Following that, because all layers of the ViT encoder use a constant latent vector size  $D$ , we flatten the  $u$  unmasked patches and transform them to  $D$  dimensions using a trainable linear projection, as shown below:

$$\mathbf{z}_0 = [X_U^1 \mathbf{E}; X_U^2 \mathbf{E}; \dots; X_U^u \mathbf{E}] + \mathbf{E}_{\text{pos}}, \quad (1)$$

where  $\mathbf{E} \in \mathbb{R}^{(T^2 \times C) \times D}$  denotes the patch embeddings and  $\mathbf{E}_{\text{pos}} \in \mathbb{R}^{(u \times D)}$  denotes the position embeddings. Position embeddings  $\mathbf{E}_{\text{pos}}$  are appended to the patch embeddings  $\mathbf{E}$  to preserve positional information. We employ learnable one-dimensional position embeddings, and the got sequence of embedding vectors  $\mathbf{z}_0$  is input to the ViT encoder. The ViT encoder has a total number of  $L$  blocks. Each block is made up of a multi-head self-attention (MSA) module, as well as a multilayer perceptron (MLP), layer normalization (LN), and residual connections. Each layer of the MLP has a Gaussian error linear unit

activation function. The global average pooling (GAP) is used to compute the final output embeddings  $\mathbf{y}$  of unmasked patches  $X_U$ . The embedding process is defined as follows:

$$\hat{\mathbf{z}}_l = \text{MSA}(\text{LN}(\mathbf{z}_{l-1})), \quad l = 1 \dots L \quad (2)$$

$$\mathbf{z}_l = \text{MLP}(\text{LN}(\hat{\mathbf{z}}_l)), \quad l = 1 \dots L \quad (3)$$

$$\mathbf{y} = \text{GAP}(\text{LN}(\mathbf{z}_L)). \quad (4)$$

The ViT decoder is an inverse version of the ViT encoder. The inputs of the ViT decoder are final output embeddings  $\mathbf{y}$  and masked tokens. The ViT decoder is only used in the pretraining process and can be designed differently from the ViT encoder. The representations learned by the MIM are also well when using a lightweight ViT decoder with fewer layers, and it can significantly decrease the network parameters and pretraining time [10].

### 3.3. Pretraining Process

Finally, by predicting the pixel values of masked patches, and RGMIM reconstructs the original patches  $X_M$ . Each element in the ViT decoder output is a vector of pixel values representing a patch. Following the ViT decoder, a linear projection layer with the number of output channels equal to the number of pixel values in a patch is added. And the ViT decoder's outputs are reshaped to generate reconstructed patches  $Y_M$ . We calculate the  $L_2$  error between the reconstructed patches  $Y_M$  and original patches  $X_M$  in the pixel-level as follows:

$$\mathcal{L} = \frac{1}{m \times T^2 \times C} \|Y_M - X_M\|_2^2, \quad (5)$$

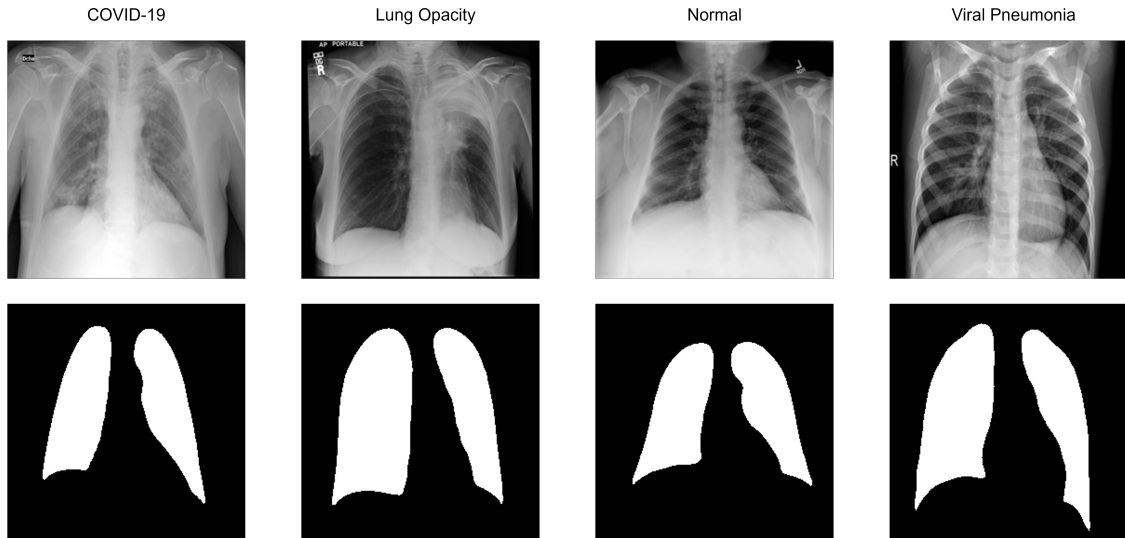


Figure 3: Examples of lung X-ray images and their corresponding masks.

where  $m \times T^2 \times C$  denotes the number of elements in original patches. As a self-supervised pretraining process, the ViT encoder can learn discriminative representations from non-labeled lung X-ray images.

### 3.4. Fine-Tuning and lung disease detection

The ViT decoder is discarded following the RGMIM pretraining process, and the pretrained ViT encoder with a linear classification layer is used to fine-tune labeled lung X-ray images using the cross-entropy loss. Given unknown lung X-ray images, the fine-tuned ViT encoder with a linear classification layer can predict the categories of the input lung X-ray images and perform lung disease detection during the test phase. Since the ViT encoder has learned discriminative representations from lung X-ray images, the fine-tuning process can be important shortened and still achieve great detection accuracy with limited labeled lung X-ray images.

## 4. Experiments

In this section, we perform extensive experiments and hyperparameter studies to validate RGMIM’s effectiveness. The dataset and settings are depicted in subsection 3.1. The findings and analysis are presented in subsection 3.2.

### 4.1. Dataset and Settings

The dataset used in our study is an open lung X-ray image dataset [49]. lung X-ray images were gathered from a variety of publicly available datasets, online sources, and published articles. Each lung X-ray image has a corresponding lung mask image. Figure 3 shows examples of lung X-ray images and their corresponding masks. The lung mask images are confirmed by expert radiologists as ground truth. The open dataset has 21,165 lung X-ray images with four classes. We randomly choose 80% of the lung X-ray images in each category as the training set (i.e., 16,933 images) and the remaining 20% as the test set (i.e.,

Table 1: Hyperparameters of the proposed method.

Hyperparameter	Value
Pretraining epoch	40
Fine-tuning epoch	30
Batch size	256
Base Learning rate	1.5e-4
Weight decay	0.05
Momentum $\beta_1$	0.9
Momentum $\beta_2$	0.95
Patch size $T$	16
Masking ration $\sigma$	75%

4,232 images). All lung X-ray images are gray-scale and are resized to  $224 \times 224$  pixels. All lung X-ray images without label data in the training set were employed for the pretraining process. The experiments were performed on an NVIDIA RTX A6000 GPU with 48G memory and employed the PyTorch framework. In our method, pre-training and fine-tuning take about 53 and 21 minutes, respectively.

As comparison methods, we used five SOTA self-supervised learning methods as comparative methods, including masked autoencoder (MAE) [10], self-knowledge distillation based self-supervised learning (SKD) [47], cross-view self-supervised learning (Cross) [48], bootstrap your own latent (BYOL) [20], and simple siamese self-supervised learning (SimSiam) [21]. As baseline methods, Transfer learning (fine-tuning from ImageNet [50]) and training from scratch were used, i.e., Transfer and From Scratch. For RGMIM and MAE, we employed the same settings in all experiments, except for the masking strategy. For example, we employed ViT-Base [25] as the ViT encoder and AdamW [51] as the optimizer. ViT-Base is a small ViT model with layer  $L = 12$ , latent vector size  $D = 768$ , 12 heads, and 3072 MLP, which often corresponds to ResNet-50 [52]. The ViT decoder employed in our experiments

Table 2: lung disease detection accuracy of different fine-tuning data volumes.

Method	Architecture	1%	5%	10%	50%	100%
RGMIM	ViT-Base	<b>0.771</b>	<b>0.893</b>	<b>0.919</b>	<b>0.957</b>	<b>0.962</b>
MAE [10]	ViT-Base	0.754	0.875	0.903	0.948	0.956
SKD [47]	ResNet-50	0.742	0.812	0.896	0.947	0.957
Cross [48]	ResNet-50	0.747	0.795	0.817	0.934	0.953
BYOL [20]	ResNet-50	0.683	0.754	0.790	0.933	0.954
SimSiam [21]	ResNet-50	0.623	0.700	0.781	0.929	0.949
Transfer	ViT-Base	0.689	0.861	0.893	0.940	0.953
Transfer	ResNet-50	0.539	0.619	0.665	0.913	0.936
From Scratch	ViT-Base	0.413	0.580	0.645	0.810	0.848
From Scratch	ResNet-50	0.284	0.496	0.532	0.619	0.774

Table 3: Hyperparameter studies on masking ratio.

Method	Masking ratio	Accuracy
RGMIM	0.15	0.949
	0.30	0.953
	0.45	0.955
	0.60	0.958
	0.75	<b>0.962</b>
	0.90	0.957
MAE [10]	0.15	0.936
	0.30	0.942
	0.45	0.947
	0.60	0.951
	0.75	<b>0.956</b>
	0.90	0.953

has layer  $L = 8$ , latent vector size  $D = 512$ , and the number of heads is 16. More details about hyperparameters are depicted in Table 1.

For SKD, Cross, BYOL, and SimSiam, we employed ResNet-50 as the backbone network. All of these contrastive learning methods make use of standard data augmentations (e.g., flipping, resizing, cropping, Gaussian blur). For Transfer and From Scratch, we used both ViT-Base and ResNet-50. To test RGMIM’s effectiveness in different training data volumes, we also randomly selected data at 1%, 5%, 10%, and 50% of the total dataset size for fine-tuning, with the ratio selected in each category being the same. Because the information density of the image is lower than language, different from the MLM employing a low masking ratio (e.g., 0.15), we set the masking ratio  $\sigma$  to 0.75 for lung X-ray images. We also studied the masking ratio for RGMIM and MAE using hyperparameters. We used a four-class accuracy as the evaluation metric.

#### 4.2. Experimental Results

The lung disease detection accuracy in different training data volumes is displayed in Table 2. Table 2 shows that RGMIM outperformed other comparative methods, achieving 0.962 detection accuracy when using the entire training set. Specifically, compared to other methods, RGMIM significantly improved lung disease detection in small data volumes, such as

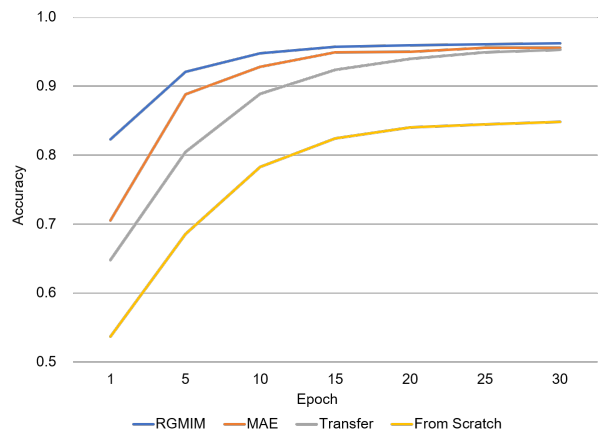


Figure 4: lung disease detection accuracy as fine-tuning epoch number increases. All methods use the ViT-Base model.

5% and 10% of the training set (846 and 1,693 images), and achieved 0.957 detection accuracy even for 50% of the training set. We can see from Table 2 that the knowledge learned by RGMIM is useful for self-supervised learning on lung X-ray images and improves representation learning performance for lung disease detection. Table 3 reveals the lung disease detection accuracy of RGMIM and MAE when employing different masking ratios. From Table 3, when the masking ratio  $\sigma = 0.75$ , the best lung disease detection accuracy is achieved, indicating that the proper masking ratio can improve the detection accuracy of both methods. In addition, we observe that RGMIM outperforms MAE in terms of robustness, especially when the masking ratio is relatively low, demonstrating the superiority of our proposed method in handling incomplete lung X-ray images.

In Figure 4, we present the accuracy changes of RGMIM when using all lung X-ray images for fine-tuning. The results indicate that RGMIM exhibits superior accuracy and faster convergence speed compared to MAE. Specifically, after only ten epochs of learning, the detection accuracy of RGMIM has already begun to converge, while MAE is still in the process of convergence. The observed difference in convergence speed between RGMIM and MAE can be attributed to the fact that RGMIM incorporates the spatial information of lung X-ray im-

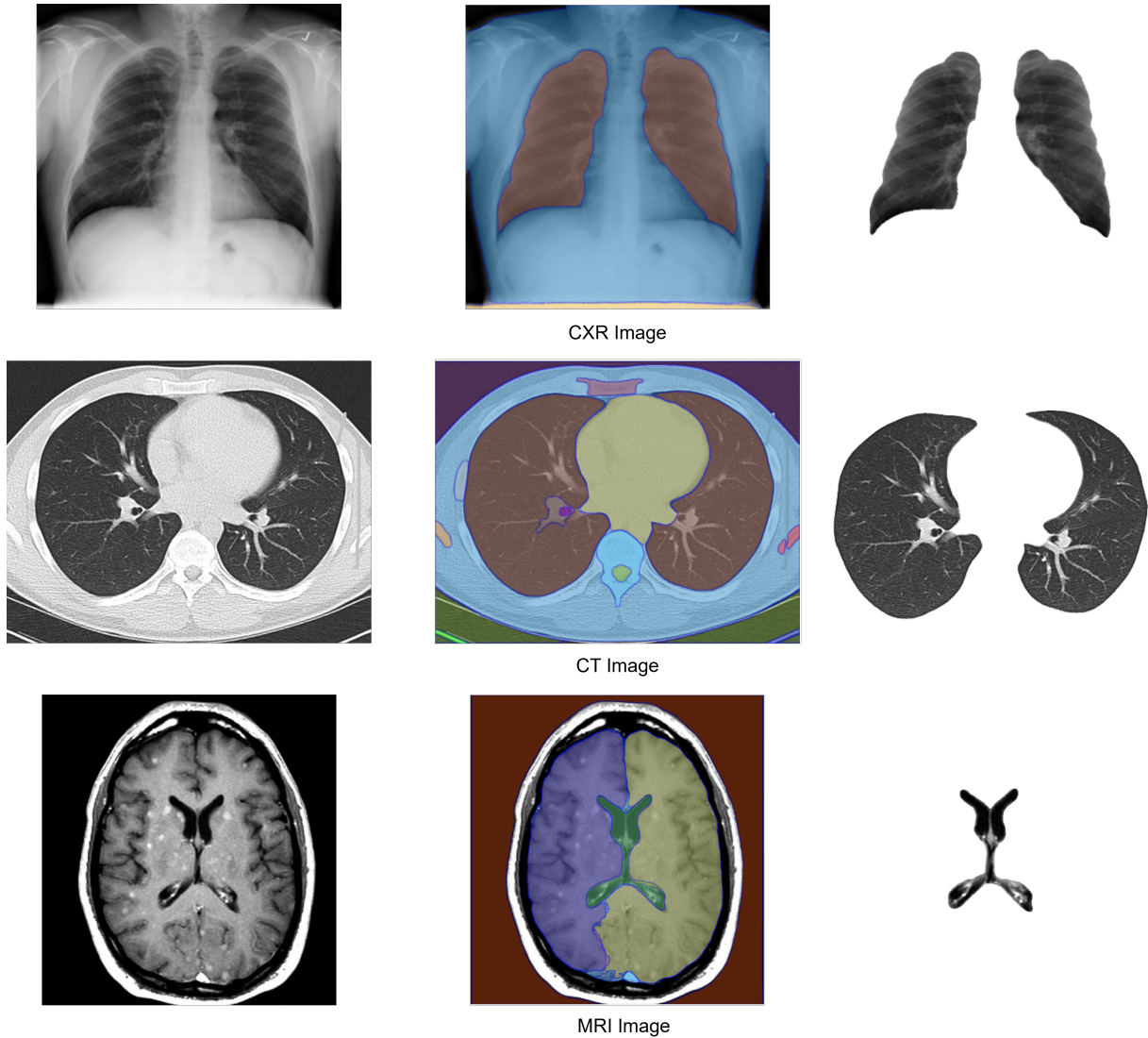


Figure 5: Segmentation results of three modality medical images by SAM.

ages through the region-guided masking strategy, which helps it to focus on the most informative regions of the images during training. Consequently, RGMIM can achieve higher accuracy with fewer iterations, making it an efficient and practical solution for lung disease detection from lung X-ray images.

## 5. Discussion

Our findings reveal the effectiveness of RGMIM for lung disease detection from lung X-ray images. RGMIM outperformed other SOTA methods significantly when fine-tuning with a small amount of labeled training data. Because of the vastly different infection statuses, medical resources, and data-sharing policies of medical images in various countries and cities, there is a likely risk of limited labeled training data [53]. Nonetheless, RGMIM can still be added to this case for high-accuracy lung disease detection.

Furthermore, RGMIM has the potential to be employed in other medical images that have a small region of interest. The

proposed RGMIM approach is designed to utilize the ground truth mask image to effectively locate the relevant information within lung X-ray images. However, in the case of other medical images with different modalities, obtaining corresponding ground truth mask images may not be feasible. To address this issue, we investigate the potential of utilizing the recently proposed Segment Anything Model (SAM) [16], a state-of-the-art technique for zero-shot image segmentation in real-world scenarios. Specifically, we apply SAM to three different modalities, namely lung X-ray, CT, and MRI, and assess the quality of the segmentation results. The segmentation results are presented in Fig. 5, where it can be observed that SAM is capable of accurately segmenting the regions of interest for each of the different modalities. The successful application of SAM to segment medical images of different modalities demonstrates the potential for utilizing RGMIM on these images without the need for corresponding ground truth mask images. This enables the deployment of RGMIM on a wider range of medical images and facilitates the development of more effective medical image

analysis techniques.

RGMIM also has some limitations. First, the use of additional lung mask images and a region-guided masking strategy raises the MIM computation cost slightly. Furthermore, there are some privacy protection issues in employing medical data from patients in real-world clinical situations. However, we have previously demonstrated that medical dataset distillation [54, 55, 56] improves the efficiency and security of data sharing among various medical facilities, which can be applied to RGMIM for clinical use.

## 6. Conclusion

This paper has suggested a novel RGMIM method for lung disease detection. In our method, we devise a new masking strategy that employs lung mask information to identify valid regions to learn more useful information for lung disease detection. RGMIM achieved 0.962 detection accuracy on an open lung X-ray dataset, according to experimental results. Furthermore, when limited training data was used, RGMIM outperformed other SOTA self-supervised learning significantly. RGMIM also has the potential to be applied to other medical images. Despite the promising experimental results, RGMIM should be tested on other medical image datasets for any potential bias.

## Ethical approval

No ethics approval is required.

## Declaration of competing interest

None declared.

## Acknowledgments

This research was supported in part by the MEXT Doctoral Program for Data-Related Innovation Expert Hokkaido University (D-DRIVE-HU) Program, AMED Grant Number JP21zf0127004, and the Hokkaido University-Hitachi Collaborative Education and Research Support Program. All experiments were conducted on the Data Science Computing System of Education and Research Center for Mathematical and Data Science, Hokkaido University.

## References

- [1] L. Chen, P. Bentley, K. Mori, K. Misawa, M. Fujiwara, D. Rueckert, Self-supervised learning for medical image analysis using image context restoration, *Medical Image Analysis* 58 (2019) 101539 (2019).
- [2] R. Krishnan, P. Rajpurkar, E. J. Topol, Self-supervised learning in medicine and healthcare, *Nature Biomedical Engineering* (2022) 1–7 (2022).
- [3] S. Shurab, R. Duwairi, Self-supervised learning methods and applications in medical imaging analysis: A survey, *PeerJ Computer Science* 8 (2022) e1045 (2022).
- [4] S. Gidaris, P. Singh, N. Komodakis, Unsupervised representation learning by predicting image rotations, in: *Proceedings of the International Conference on Learning Representations (ICLR)*, 2018 (2018).
- [5] M. Noroozi, P. Favaro, Unsupervised learning of visual representations by solving jigsaw puzzles, in: *Proceedings of the European Conference on Computer Vision (ECCV)*, 2016, pp. 69–84 (2016).
- [6] X. Liu, F. Zhang, Z. Hou, L. Mian, Z. Wang, J. Zhang, J. Tang, Self-supervised learning: Generative or contrastive, *IEEE Transactions on Knowledge and Data Engineering* (2021).
- [7] T. Chen, S. Kornblith, M. Norouzi, G. Hinton, A simple framework for contrastive learning of visual representations, in: *Proceedings of the International Conference on Machine Learning (ICML)*, 2020 (2020).
- [8] G. Li, R. Togo, T. Ogawa, M. Haseyama, Tribyol: Triplet byol for self-supervised representation learning, in: *Proceedings of the IEEE International Conference on Acoustics, Speech and Signal Processing (ICASSP)*, 2022, pp. 3458–3462 (2022).
- [9] H. Bao, L. Dong, F. Wei, Beit: Bert pre-training of image transformers, in: *Proceedings of the International Conference on Learning Representations (ICLR)*, 2022 (2022).
- [10] K. He, X. Chen, S. Xie, Y. Li, P. Dollár, R. Girshick, Masked autoencoders are scalable vision learners, in: *Proceedings of the IEEE/CVF Conference on Computer Vision and Pattern Recognition (CVPR)*, 2022, pp. 16000–16009 (2022).
- [11] Z. Xie, Z. Zhang, Y. Cao, Y. Lin, J. Bao, Z. Yao, Q. Dai, H. Hu, Simsim: A simple framework for masked image modeling, in: *Proceedings of the IEEE/CVF Conference on Computer Vision and Pattern Recognition (CVPR)*, 2022, pp. 9653–9663 (2022).
- [12] J. Devlin, M.-W. Chang, K. Lee, K. Toutanova, Bert: Pre-training of deep bidirectional transformers for language understanding, in: *Proceedings of the Annual Conference of the North American Chapter of the Association for Computational Linguistics (NAACL)*, 2019 (2019).
- [13] C. Wei, H. Fan, S. Xie, C.-Y. Wu, A. Yuille, C. Feichtenhofer, Masked feature prediction for self-supervised visual pre-training, in: *Proceedings of the IEEE/CVF Conference on Computer Vision and Pattern Recognition (CVPR)*, 2022, pp. 14668–14678 (2022).
- [14] Z. Chen, D. Agarwal, K. Aggarwal, W. Safta, M. M. Balan, K. Brown, Masked image modeling advances 3d medical image analysis, in: *Proceedings of the IEEE/CVF Winter Conference on Applications of Computer Vision (WACV)*, 2023, pp. 1969–1979 (2023).
- [15] H.-C. Shin, H. R. Roth, M. Gao, L. Lu, Z. Xu, I. Nogues, J. Yao, D. Molur, R. M. Summers, Deep convolutional neural networks for computer-aided detection: Cnn architectures, dataset characteristics and transfer learning, *IEEE Transactions on Medical Imaging* 35 (5) (2016) 1285–1298 (2016).
- [16] A. Kirillov, E. Mintun, N. Ravi, H. Mao, C. Rolland, L. Gustafson, T. Xiao, S. Whitehead, A. C. Berg, W.-Y. Lo, P. Dollár, R. Girshick, Segment anything, *arXiv:2304.02643* (2023).
- [17] L. Jing, Y. Tian, Self-supervised visual feature learning with deep neural networks: A survey, *IEEE Transactions on Pattern Analysis and Machine Intelligence* (2020).
- [18] R. D. Hjelm, A. Fedorov, S. Lavoie-Marchildon, K. Grewal, P. Bachman, A. Trischler, Y. Bengio, Learning deep representations by mutual information estimation and maximization, in: *Proceedings of the International Conference on Learning Representations (ICLR)*, 2019 (2019).
- [19] K. He, H. Fan, Y. Wu, S. Xie, R. Girshick, Momentum contrast for unsupervised visual representation learning, in: *Proceedings of the IEEE/CVF Conference on Computer Vision and Pattern Recognition (CVPR)*, 2020, pp. 9729–9738 (2020).
- [20] J.-B. Grill, F. Strub, F. Altché, C. Tallec, P. Richemond, E. Buchatskaya, C. Doersch, B. Avila Pires, Z. Guo, M. Gheshlaghi Azar, B. Piot, K. Kavukcuoglu, R. Munos, M. Valko, Bootstrap your own latent—a new approach to self-supervised learning, in: *Proceedings of the Advances in Neural Information Processing Systems (NeurIPS)*, 2020, pp. 21271–21284 (2020).
- [21] X. Chen, K. He, Exploring simple siamese representation learning, in: *Proceedings of the IEEE/CVF Conference on Computer Vision and Pattern Recognition (CVPR)*, 2021, pp. 15750–15758 (2021).
- [22] C. Zhang, C. Zhang, J. Song, J. S. K. Yi, K. Zhang, I. S. Kweon, A survey on masked autoencoder for self-supervised learning in vision and beyond, *arXiv preprint arXiv:2208.00173* (2022).
- [23] J. T. Rolfe, Discrete variational autoencoders, in: *Proceedings of the*

- International Conference on Learning Representations (ICLR), 2017 (2017).
- [24] P. Vincent, H. Larochelle, Y. Bengio, P.-A. Manzagol, Extracting and composing robust features with denoising autoencoders, in: Proceedings of the International Conference on Machine Learning (ICML), 2008, pp. 1096–1103 (2008).
- [25] A. Dosovitskiy, L. Beyer, A. Kolesnikov, D. Weissenborn, X. Zhai, T. Unterthiner, M. Dehghani, M. Minderer, G. Heigold, S. Gelly, J. Uszkoreit, N. Houlsby, An image is worth 16x16 words: Transformers for image recognition at scale, in: Proceedings of the International Conference on Learning Representations (ICLR), 2021 (2021).
- [26] M. Chen, A. Radford, R. Child, J. Wu, H. Jun, D. Luan, I. Sutskever, Generative pretraining from pixels, in: Proceedings of the International Conference on Machine Learning (ICML), PMLR, 2020, pp. 1691–1703 (2020).
- [27] S. K. Zhou, H. Greenspan, C. Davatzikos, J. S. Duncan, B. Van Ginneken, A. Madabhushi, J. L. Prince, D. Rueckert, R. M. Summers, A review of deep learning in medical imaging: Imaging traits, technology trends, case studies with progress highlights, and future promises, Proceedings of the IEEE 109 (5) (2021) 820–838 (2021).
- [28] A. Hosny, C. Parmar, J. Quackenbush, L. H. Schwartz, H. J. Aerts, Artificial intelligence in radiology, Nature Reviews Cancer 18 (8) (2018) 500–510 (2018).
- [29] S. Chilamkurthy, R. Ghosh, S. Tanamala, M. Biviji, N. G. Campeau, V. K. Venugopal, V. Mahajan, P. Rao, P. Warier, Deep learning algorithms for detection of critical findings in head ct scans: a retrospective study, The Lancet 392 (10162) (2018) 2388–2396 (2018).
- [30] G. Mohan, M. M. Subashini, Mri based medical image analysis: Survey on brain tumor grade classification, Biomedical Signal Processing and Control 39 (2018) 139–161 (2018).
- [31] D. Ahmedt-Aristizabal, M. A. Armin, S. Denman, C. Fookes, L. Petersson, A survey on graph-based deep learning for computational histopathology, Computerized Medical Imaging and Graphics 95 (2022) 102027 (2022).
- [32] S. M. Anwar, M. Majid, A. Qayyum, M. Awais, M. Alnowami, M. K. Khan, Medical image analysis using convolutional neural networks: a review, Journal of medical systems 42 (2018) 1–13 (2018).
- [33] O. Jimenez-del Toro, S. Otálora, M. Andersson, K. Eurén, M. Hedlund, M. Rousson, H. Müller, M. Atzori, Analysis of histopathology images: From traditional machine learning to deep learning, in: Biomedical Texture Analysis, Elsevier, 2017, pp. 281–314 (2017).
- [34] X. Xie, J. Niu, X. Liu, Z. Chen, S. Tang, S. Yu, A survey on incorporating domain knowledge into deep learning for medical image analysis, Medical Image Analysis 69 (2021) 101985 (2021).
- [35] P. Celard, E. Iglesias, J. Sorribes-Fdez, R. Romero, A. S. Vieira, L. Borrajo, A survey on deep learning applied to medical images: from simple artificial neural networks to generative models, Neural Computing and Applications 35 (3) (2023) 2291–2323 (2023).
- [36] Z. Chen, S. Chen, Y. Wu, Y. Qian, C. Wang, S. Liu, Y. Qian, M. Zeng, Large-scale self-supervised speech representation learning for automatic speaker verification, in: Proceedings of the IEEE International Conference on Acoustics, Speech and Signal Processing (ICASSP), IEEE, 2022, pp. 6147–6151 (2022).
- [37] W. L. Bi, A. Hosny, M. B. Schabath, M. L. Giger, N. J. Birkbak, A. Mehrtash, T. Allison, O. Arnaout, C. Abbosh, I. F. Dunn, et al., Artificial intelligence in cancer imaging: clinical challenges and applications, CA: A Cancer Journal for Clinicians 69 (2) (2019) 127–157 (2019).
- [38] A. Chatsias, T. Joyce, G. Papanastasiou, S. Semple, M. Williams, D. E. Newby, R. Dharmakumar, S. A. Tsaftaris, Disentangled representation learning in cardiac image analysis, Medical Image Analysis 58 (2019) 101535 (2019).
- [39] Z. Zhou, V. Sodha, J. Pang, M. B. Gotway, J. Liang, Models genesis, Medical Image Analysis 67 (2021) 101840 (2021).
- [40] Y. Tang, D. Yang, W. Li, H. R. Roth, B. Landman, D. Xu, V. Nath, A. Hatamizadeh, Self-supervised pre-training of swin transformers for 3d medical image analysis, in: Proceedings of the IEEE/CVF Conference on Computer Vision and Pattern Recognition (CVPR), 2022, pp. 20730–20740 (2022).
- [41] K. Chaitanya, E. Erdil, N. Karani, E. Konukoglu, Contrastive learning of global and local features for medical image segmentation with limited annotations, Proceedings of the Advances in Neural Information Processing Systems (NeurIPS) 33 (2020) 12546–12558 (2020).
- [42] L. Zhou, H. Liu, J. Bae, J. He, D. Samaras, P. Prasanna, Self pre-training with masked autoencoders for medical image analysis, arXiv preprint arXiv:2203.05573 (2022).
- [43] X. Li, X. Hu, X. Qi, L. Yu, W. Zhao, P.-A. Heng, L. Xing, Rotation-oriented collaborative self-supervised learning for retinal disease diagnosis, IEEE Transactions on Medical Imaging 40 (9) (2021) 2284–2294 (2021).
- [44] Y. Li, Q. Lao, Q. Kang, Z. Jiang, S. Du, S. Zhang, K. Li, Self-supervised anomaly detection, staging and segmentation for retinal images, Medical Image Analysis 87 (2023) 102805 (2023).
- [45] X. Wang, R. Su, W. Xie, W. Wang, Y. Xu, R. Mann, J. Han, T. Tan, 2.75 d: Boosting learning by representing 3d medical imaging to 2d features for small data, Biomedical Signal Processing and Control 84 (2023) 104858 (2023).
- [46] G. Li, R. Togo, T. Ogawa, M. Haseyama, Boosting automatic covid-19 detection performance with self-supervised learning and batch knowledge ensembling, Computers in Biology and Medicine 158 (2023) 106877 (2023).
- [47] G. Li, R. Togo, T. Ogawa, M. Haseyama, Self-knowledge distillation based self-supervised learning for covid-19 detection from chest x-ray images, in: Proceedings of the IEEE International Conference on Acoustics, Speech and Signal Processing (ICASSP), 2022, pp. 1371–1375 (2022).
- [48] G. Li, R. Togo, T. Ogawa, M. Haseyama, Covid-19 detection based on self-supervised transfer learning using chest x-ray images, International Journal of Computer Assisted Radiology and Surgery (2022) 1–8 (2022).
- [49] T. Rahman, A. Khandakar, Y. Qiblawey, A. Tahir, S. Kiranyaz, S. B. A. Kashem, M. T. Islam, S. Al Maadeed, S. M. Zughaier, M. S. Khan, M. E. H. Chowdhury, Exploring the effect of image enhancement techniques on covid-19 detection using chest x-ray images, Computers in Biology and Medicine 132 (2021) 104319 (2021).
- [50] J. Deng, W. Dong, R. Socher, L.-J. Li, K. Li, L. Fei-Fei, Imagenet: A large-scale hierarchical image database, in: Proceedings of the IEEE Conference on Computer Vision and Pattern Recognition (CVPR), 2009, pp. 248–255 (2009).
- [51] I. Loshchilov, F. Hutter, Decoupled weight decay regularization, in: Proceedings of the International Conference on Learning Representations (ICLR), 2019 (2019).
- [52] K. He, X. Zhang, S. Ren, J. Sun, Deep residual learning for image recognition, in: Proceedings of the IEEE/CVF Conference on Computer Vision and Pattern Recognition (CVPR), 2016, pp. 770–778 (2016).
- [53] J. Shuja, E. Alanazi, W. Alasmay, A. Alashaikh, Covid-19 open source data sets: a comprehensive survey, Applied Intelligence 51 (2021) 1296–1325 (2021).
- [54] G. Li, R. Togo, T. Ogawa, M. Haseyama, Soft-label anonymous gastric x-ray image distillation, in: Proceedings of the IEEE International Conference on Image Processing (ICIP), 2020, pp. 305–309 (2020).
- [55] G. Li, R. Togo, T. Ogawa, M. Haseyama, Compressed gastric image generation based on soft-label dataset distillation for medical data sharing, Computer Methods and Programs in Biomedicine 227 (2022) 107189 (2022).
- [56] G. Li, R. Togo, T. Ogawa, M. Haseyama, Dataset distillation for medical dataset sharing, in: Proceedings of the AAAI Conference on Artificial Intelligence (AAAI), Workshop, 2023, pp. 1–6 (2023).